Growth of Ordered Hexakis-dodecyl-hexabenzocoronene Layers from Solution: A SFM and ARUPS Study

ARTICLE *in* THE JOURNAL OF PHYSICAL CHEMISTRY B · OCTOBER 2001

Impact Factor: 3.3 · DOI: 10.1021/jp004076t

Growth of Ordered Hexakis-dodecyl-hexabenzocoronene Layers from Solution: A SFM and ARUPS Study

Paolo Samorí,[†] Matthias Keil,[‡] Rainer Friedlein,[‡] Jonas Birgerson,[‡] Mark Watson,[§] Klaus Müllen,[§] William R. Salaneck,*[,‡] and Jürgen P. Rabe*[,†]

Department of Physics, Humboldt University Berlin, Invalidenstrasse 110, 10115 Berlin, Germany, Department of Physics, IFM, Linköping University, S-581 83 Linköping, Sweden, and Max-Planck-Institute for Polymer Research, Ackermannweg 10, 55021 Mainz, Germany

Received: November 7, 2000; In Final Form: July 3, 2001

The layer growth of a polycyclic aromatic hydrocarbon moiety, hexakis-dodecyl-hexabenzocoronene (HBC-C_{12}), from solution onto a conductive flat solid substrate has been studied. Scanning Force Microscopy (SFM), together with the analysis of the intensities of π-structures in spectra of Angle-Resolved Ultraviolet Photoelectron Spectroscopy (ARUPS) measurements, revealed that the HBC-C_{12} molecules can self-assemble as dry layers with the conjugated disklike molecules lying flat on the (0001) plane of highly oriented pyrolitic graphite (HOPG). By varying the rate of the molecular physisorption it was possible to orient these molecular architectures along preferential directions according to the symmetry of the substrate. Additionally, the film morphology is affected by the concentration of the solution. This indicates that the growth of these organic layers on HOPG is a kinetically governed process which, if carried out sufficiently slowly, leads to the growth of hetero-epitaxial crystallites.

Introduction

Structurally well-defined and stable molecular architectures, not involving covalent bonds, may be prepared by exploiting the self-assembly of molecules, at the solid−liquid interface under equilibrium conditions.[1] This approach can be employed to grow also *dry* highly ordered thin films of large organic (macro)molecules that, because of their size, cannot be processed by vacuum sublimation.[2,3] On the other hand, conjugated polymers and oligomers have gained a great deal of attention in the last two decades because of their physical and chemical properties that render them candidates for active components in optoelectronic devices.[4−8] The performance of these devices is strongly dependent on the interplay between electronic structure and molecular arrangement.[7−16] By combining chemically sensitive techniques such as photoelectron spectroscopies with the spatial resolution of Scanning Probe Microscopies it is possible to investigate both these properties. Physisorbed monolayers of a soluble synthetic disklike "nano-graphene" molecule, namely hexakis-dodecyl-hexabenzocoronene (HBC-C_{12})[17−19] and larger allotropes[20] have already been studied at the solid−liquid interface with STM. A diode-like electrical behavior due to the conjugated moiety in the gap has been observed with Scanning Tunneling Spectroscopy.[17] In the present work, the growth of dry layers (namely, at the solid−air interface for SFM studies and at the solid−vacuum in the case of photoelectron spectroscopy ones) from solutions of HBC-C_{12} (Figure 1) is investigated. These layered-architectures were characterized by means of Scanning Force Microscopy (SFM) in Tapping Mode and Angle-Resolved Ultraviolet Photoelectron Spectroscopy (ARUPS) using polarized synchrotron radiation. X-ray Photoelectron Spectroscopy (XPS) was employed to determine the stoichiometry of the films.

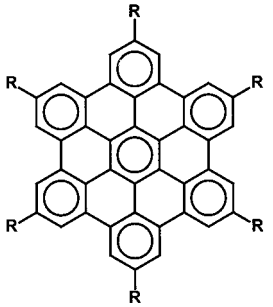

Figure 1. Chemical structure of HBC-C_{12}.

Experimental Procedures

The synthesis of hexakis-dodecyl-hexabenzocoronene (HBC-C_{12}) (Figure 1) has been described elsewhere.[18] Samples have been prepared by applying a drop of 20 μL of a solution of HBC-C_{12} in 1,2,-trichlorobenzene (boiling temperature 487 K, Aldrich) on the basal plane of a freshly cleaved Highly Oriented Pyrolitic Graphite (HOPG) substrate (Advanced ceramics Corp., grade ZYH). To permit the evaporation of the solvent and the molecular assembling to occur at decreasing rates the thin films were grown following different methods:

(A) spin coating for 30 s with a velocity of 5000 rounds/min;

(B) fast solution casting: the wet sample was stored in air, not saturated with the vapor of its own solution during the solvent evaporation and progress of solidification; or

* Authors to whom correspondence should be addressed: Prof. Dr. J. P. Rabe (Fax: +49-30-20937632. E-mail: rabe@physik.hu-berlin.de) and Prof. Dr. W. R. Salaneck (Fax: +46-13-137568. E-mail: wrs@ifm.liu.se).
[†] Humboldt University Berlin.
[‡] Linköping University.
[§] Max-Planck-Institute for Polymer Research.

10.1021/jp004076t CCC: $20.00
Published on Web 10/19/2001

(C) slow solution casting: the wet sample was located in an air environment saturated with the vapor of the organic solution during the solvent evaporation and progress of solidification.

The time periods for these processes were 3 min, 3−5 h, and 12 h, respectively. The last type (C) took over 12 h. Concentrations of the solutions for films prepared by solution casting (B and C) were chosen such that the HOPG could be coated approximately with one layer, assuming a packing as determined by STM at the liquid−graphite interface, namely, with the disklike molecules lying flat on the substrate.[17] On the other hand, the films produced by spin coating possess a nominal thickness of a few tens of layers.

The film morphologies were studied by Tapping Mode−Scanning Force Microscopy,[21,22] recording both the height signal (output of the feedback signal) and the phase signal (phase lag of the oscillation relative to the driver). While the first types of images provide topographical maps of the surface, the latter are extremely sensitive to structural heterogeneities on the sample surface.[23] The SFM Nanoscope III[24] was run in an air environment at room temperature with scan rates of 1−3 Hz/line. A range of scan lengths between 1 and 120 μm, with a resolution of 512 × 512 pixels, were explored using the E and J scanners[24] and silicon nanoprobes[24] with a spring constant of $k = 17-64$ N/m. The piezo-displacements in all three dimensions were calibrated by imaging gold calibration grids and freshly cleaved muscovite mica surfaces. The step heights were measured quantitatively from single profiles using the software of the Nanoscope III. An average error bar of ±0.02−0.03 nm on the obtained values should be taken into account.

The contour size of the molecule was computed using molecular mechanics calculations.[25] The diameter of the HBC-C_{12}, in the case where the alkyl side chains are in their fully extended conformations, is about 4.0 nm. The van der Waals thickness of the conjugated, planar aromatic core amounts to 0.355 nm.[25]

X-ray photoelectron spectroscopy (XPS) has been carried out using a home designed and built, ultrahigh vacuum (UHV) apparatus with a base pressure of better than 1×10^{-9} mbar. Unfiltered Mg Kα radiation (1254.6 eV) was used. The surface compositions of the films confirmed the overall purity of the adsorbate, with the exception of a small quantity of residual oxygen (C/O = 0.98). Since no further information besides the C/O ratio can be deduced from these data, the XPS results are not shown here. Thermal annealing of the samples has been performed inside the ultrahigh vacuum chamber of the spectrometer.

The ARUPS investigation has been carried out, on the films as prepared and after thermal annealing for 1 h at 425 K, using polarized synchrotron radiation of beamline I411 of MAX-II (MAX Laboratory of Synchrotron Radiation, Lund, Sweden). A detailed description of the undulator, SX700 monochromator, and end-station is given elsewhere.[26,27] A Scienta electron energy analyzer (SES200) possessing an angular resolution of approximately 1° has been employed. The analyzer and the sample are rotatable around the axis of the incident light. The angle between the incident light and the entrance of the analyzer is fixed at 90°. The angle between the incident light and the surface normal can be chosen to be 0° or 60°.

Results and Discussions

Scanning Force Microscopy images of a layer of HBC-C_{12} on HOPG are displayed in Figure 2. The layer has been prepared by spin coating, using a solution containing a quantity of HBC-C_{12}, sufficient for covering the substrate with 1000 layers

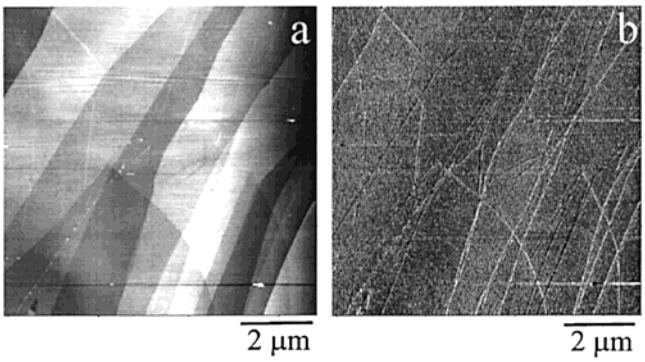

Figure 2. Tapping Mode Scanning Force Microscopy images of HBC-C_{12} film prepared by spin coating the quantity to form 1000 layers on HOPG (procedure A). Image (a) Height image: *z*-scale (*h*) = 10 nm; b) Phase image: *z*-scale = 7°.

(procedure A). However, only some of the molecules adsorb to the surface because there is a loss of material during the spinning, the amount of which cannot be quantified. The film surface exhibits a flat morphology, made up of polygonal planes extended on the micrometer scale. This structure is similar to that of the bare substrate. The steps in height between the planes are 0.34 nm, or multiples thereof, in good agreement with both the size of HOPG steps[28] and the thickness of the HBC-C_{12} molecules, if they would lie flat on the surface. Phase imaging (Figure 2b) indicates the presence of only one phase on the sample surface, which might be either an uncoated HOPG substrate or HOPG homogeneously coated with HBC-C_{12}. Complementary Scanning Tunneling Microscopy imaging studies revealed unambiguously that in these films the conductive substrate is homogeneously coated with a less conductive organic adlayer. Thus the case of an uncoated graphite substrate must be dismissed. It might be expected that, due to the fast rate of physisorption, the degree of molecular order of the organic moiety adsorbed onto the flat substrate may be small on a molecular scale. However, the interfacial roughness of this film is very small over areas on the micrometer length scale. Additionally, with valence band photoelectron spectroscopy, the characteristic π-structures of HBC-C_{12} have been recorded and compared with those of HOPG, demonstrating that the graphite surface is covered with a some-nanometers-thick adsorbate film (not shown here). On the other hand, the spin coating of a quantity of HBC-C_{12} to produce a monolayer did not show adsorbate features in the spectra. For this reason, we have investigated spin-coated thicker films, instead of monolayer thick films, as in the other following cases.

The morphology of HBC-C_{12} films obtained by "fast casting" (procedure B) is shown in Figure 3. In this case, HBC-C_{12} molecules self-assemble into inhomogeneous monolayers (small islands) with a constant height of 0.35 nm, or multiples thereof, which is consistent with a layer-by-layer growth of the HBC-C_{12} disklike molecules oriented flat on the HOPG surface.[17] Thicker domains with higher multiples of 0.35 nm, up to about 2.5 nm were also observed. The height and phase images indicate different phases on the sample surface that could be either attributed to a diverse orientation of the molecules with respect to the basal plane of the substrate, in different areas of the sample, or to an only partially coated HOPG surface. The molecular assembly displayed in Figure 3 is likely to represent a metastable state toward the formation of more extended clusters (layers) occurring via coalescence of these small domains.[10]

The thin films prepared by slow solution casting (method C) exhibit well-defined regions of monolayer coverage (Figure 4),

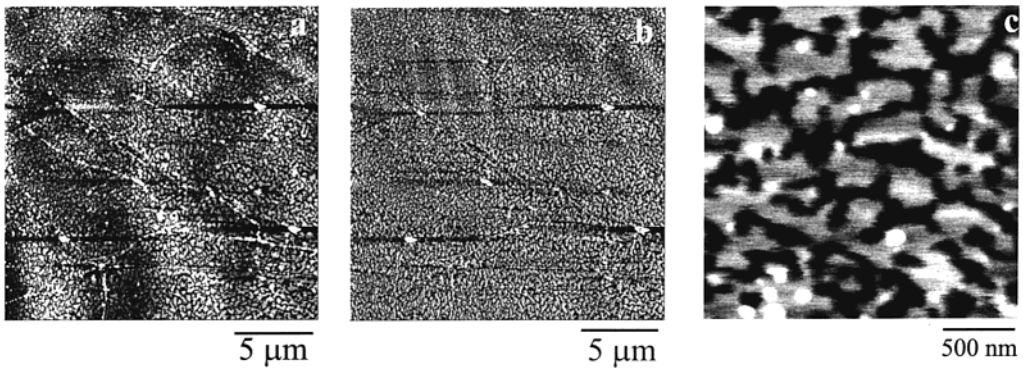

Figure 3. Tapping Mode Scanning Force Microscopy micrographs of a HBC-C_{12} surface grown by solution casting (procedure B), which results in a monolayer coverage of the HOPG substrate. (a) Height image: $h = 20$ nm; (b) Phase image: z-scale = 6°; (c) Height image: $h = 20$ nm.

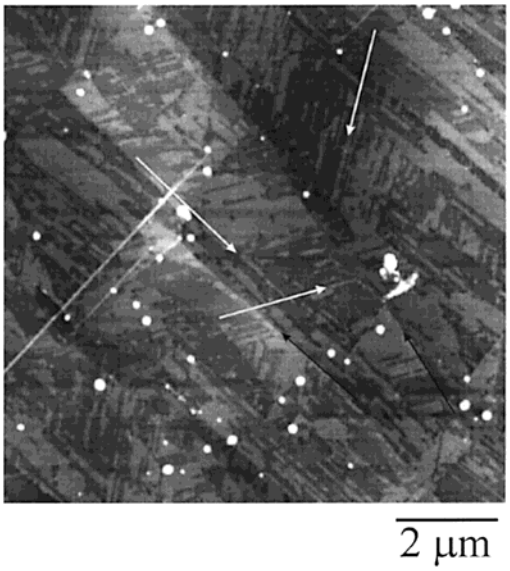

Figure 4. Topographical Tapping Mode Scanning Force Microscopy image of the surface of a film of HBC-C_{12} molecules which was produced by slow evaporation of the solvent in a controlled environment (route C). $h = 15$ nm. The white arrows indicate the preferential directions along which the anisotropic layers grow. The tilt angle between them is 60° in perfect agreement with the 3-fold symmetry of the HOPG substrate. The black arrows indicate the domain boundaries of the micrometer size crystals of the HOPG surface.

which are lying on the micrometer size single crystals of the HOPG substrate (the black arrows indicate the domain boundaries of the substrate crystallites). Interestingly, some anisotropic overlayers, namely domains extended over several hundreds of square nanometers, are assembled on the monolayers and also exhibit thicknesses of 0.35 nm. The crystallites are aligned along preferential directions (with an angle between them of 120°) according to the 3-fold symmetry of the basal plane of the crystalline HOPG substrate, marked by the white arrows in Figure 4. Such alignment, which is not induced by the domain boundaries of the underlying HOPG substrate, provides unambiguous evidence of a recognition between the lattice of the adsorbate and the one of the substrate. This indicates that these architectures are hetero-epitaxial crystallites.[29] It is worth noting that the thicknesses of a monolayer of HOPG (0.335 nm) and of HBC-C_{12} (0.355 nm) are very similar. For this reason, measurements of the thickness of domains detected from SFM topographical profiles do not allow an unambiguous identification of a given surface as adsorbate or substrate. This assignment can be achieved only with a careful observation of the shape of the boundaries and, in cases of uncertainty, by using a complementary chemically sensitive imaging mode such as Phase Imaging SFM.[23]

Applying relatively high forces in the tens of nano-newtons range with Scanning Force Microscopy in the contact mode we could easily scratch the films, by moving the upper layers of the thick film prepared by fast solution casting (procedure (B), not shown here). Nevertheless, the first layers in contact with the substrate are strongly bound to the surface, and therefore difficult to remove.[30] It is likely that in the first layer both the aliphatic parts and the aromatic part of the molecule lie flat on the basal plane of the substrate. This geometry allows a maximization of the attractive van der Waals interactions. Moreover, in this scenario, overlayers are grown onto the first layer in contact with the substrate. The degree of molecular order in the upper layers, and consequently also in the underlying layers, is expected to be higher with a decreasing rate of molecular physisorption from solution on the solid surface. The mechanism governing the formation of these HBC interfaces may be divided conceptually into three steps: (1) homogeneous coverage of the substrate with a first monolayer; (2) growth of overlayers, layer by layer; and (3) ordering of the layers along preferential directions induced by the crystalline substrate.

The first step takes place for every type of film preparation discussed above, (A) through (C). The second step, where the molecules are ordered parallel to the HOPG (0001)-plane, occurs certainly for films prepared by solution casting (B and C). The third step takes place only using a slow casting (C). Note that in both procedures (B) and (C), the molecular coverage obtained, due to the low quantity of adsorbing material, is not homogeneous over the macroscopic size (mm^2) of the sample. It turned out that these variations over large distances may be controlled to a certain extent by using the slow deposition procedure (C). In each of the three steps an important role is played by diffusional motions of the molecules. A high diffusional constant can be expected in the presence of a solvent; in slow processes such as (C) the diffusion can take place for a longer time. This molecular dynamics allows indeed the optimization of the ordering of the layers along the preferential directions.

Angle-Resolved Ultraviolet Photoelectron Spectroscopy (ARUPS) provides additional information on the molecular adsorbates. Generally, a detailed quantitative analysis of the orientation and the symmetry of an adsorbed molecule can be achieved using dipole selection rules.[31] Here, the dipole matrix element

$$M_{f,i} \propto |\langle \phi_f | \vec{\mathbf{A}} \cdot \vec{\mathbf{p}} | \phi_i \rangle|^2 \qquad (1)$$

which is derived from Fermi's Golden Rule in the dipole approximation, must be totally symmetric in order to be nonzero.

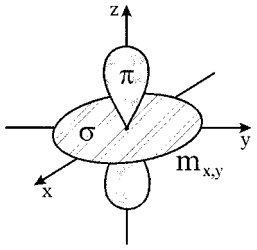

$$M_{f,i} \propto \left|\left\langle \phi_f \left| \vec{\mathbf{A}} \cdot \vec{\mathbf{p}} \right| \phi_i \right\rangle\right|^2 \quad \vec{\mathbf{A}} \parallel \vec{\mathbf{E}} \qquad (1)$$

$$\vec{E} \parallel m_{x,y} \quad \Rightarrow \quad \vec{\mathbf{A}} \cdot \vec{\mathbf{p}} \left| \phi_i^{\pi} \right\rangle = \left| odd \right\rangle \qquad (a)$$

$$\text{Detector in x,y plane} \quad \Rightarrow \quad M_{f,i} \propto \left|\left\langle even \middle| odd \right\rangle\right|^2 = 0$$

$$\vec{E} \perp m_{x,y} \quad \Rightarrow \quad \vec{\mathbf{A}} \cdot \vec{\mathbf{p}} \left| \phi_i^{\pi} \right\rangle = \left| even \right\rangle \qquad (b)$$

$$\text{Detector in x,y plane} \quad \Rightarrow \quad M_{f,i} \propto \left|\left\langle even \middle| even \right\rangle\right|^2 \neq 0$$

Figure 5. Schematic illustration of the predictions of symmetry selection rules for a lateral randomly distributed HBC-C_{12} molecule.

The initial state, ϕ_i, and the final state, ϕ_f, wave functions involve the particular orbital of the bound electron, and the emitted electron, respectively. The operator $\vec{\mathbf{A}} \cdot \vec{\mathbf{p}}$ is a product of the dipole operator $\vec{\mathbf{p}}$ and the vector potential $\vec{\mathbf{A}}$. The electric field vector $\vec{\mathbf{E}}$ of the incoming light is parallel to vector potential $\vec{\mathbf{A}}$.[32] Equation 1 shows, that, when $\vec{\mathbf{E}}$ of the incident radiation is varied with respect to the symmetry elements of the molecule—like high symmetric axis or mirror planes—the excitation from a specific initial state ϕ_i is only allowed into a final state ϕ_f, when both have a particular symmetry. In an ARUPS experiment, by determining the spatial distribution of the photoelectrons, the final state is probed. Then, by chosing the orientation of $\vec{\mathbf{E}}$ with respect to the symmetry elements of the molecule, information on the initial state is provided.

In the particular case of HBC-C_{12} films on HOPG a lateral order of the adsorbed molecules is exceptional because of the polycrystalline nature of the HOPG (0001)-surface on the hundreds of micrometers scale. Our aim was to gain insight into the orientation of the HBC disc-shaped core with respect to the basal plane of HOPG. For this purpose, the molecular plane of the HBC core can be regarded as a symmetry element, for the application of eq 1. This plane represents a mirror plane of the HBC core (see Figure 1). As outlined in Figure 5 all π-orbitals have an odd symmetry and all σ-orbitals an even symmetry with respect to this mirror plane $m_{x,y}$. Further, in Figure 5, we apply eq 1 for photoelectron emission from the π-orbitals. We show the two cases, where $\vec{\mathbf{E}}$ is oriented parallel or perpendicular the plane $m_{x,y}$, and where the detector is located in the mirror plane $m_{x,y}$. To detect a signal, then, all final states must have an even symmetry with respect to this plane. This leads to the selection rules, that $M_{f,I} \neq 0$ is only fulfilled, when $\vec{\mathbf{E}}$ of the incoming light is oriented perpendicular to the mirror plane $m_{x,y}$ (eq 1b in Figure 5).

In Figure 6 the π-regions of ARUPS spectra are shown for a film with an average monolayer thickness prepared by procedure (C). Figure 6a shows the spectra of an as-prepared and Figure 6b those of an annealed film. Figure 6c are the spectra of freshly cleaved HOPG. In each case the spectra were recorded at three different geometries, where the photon incident (α) and the electron takeoff (θ, ϕ) angles were varied. Figures 6a and 6b exhibit features at 1.5 and 2.9 eV (labeled as 1 and 2), which have been attributed to electrons emitted from groups of states with π-symmetry: peak 1 contains contributions from

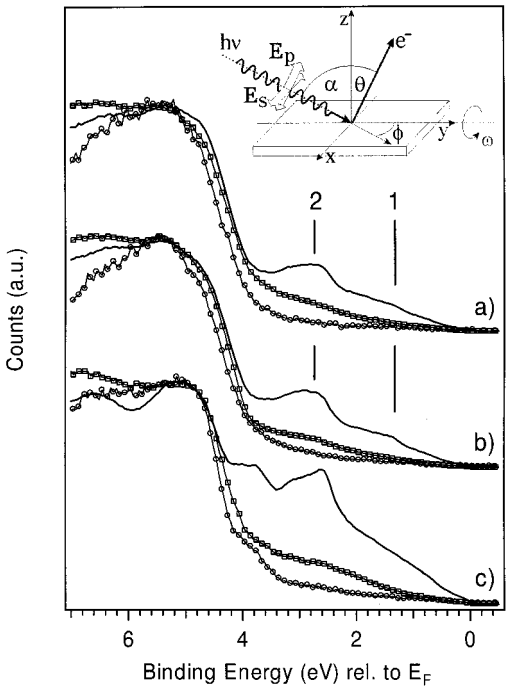

Figure 6. ARUPS spectra of samples prepared by slow casting of one layer, recorded at different geometries (solid curves: p-polarized light, $\alpha = 60°$, $\theta = 30°$, $\phi = 0°$; curves with unfilled circles: s-polarized light, $\alpha = 60°$, $\theta = 90°$, $\phi = 90°$; curves with unfilled squares: s-polarized light, $\alpha = 60°$, $\theta = 30°$, $\phi = 0°$). (a) as-prepared; (b) thermal annealed at 425 K for 1 h, and (c) of freshly cleaved HOPG. The spectra were plotted relative to the Fermi level; the photon energy was $h\nu = 85$ eV.

three different π-states, while peak 2 corresponds to a contribution of six π-states.[27] The broad unstructured features in the binding energy range above 4 eV arise from σ-states of the alkyl side chains, as well as from states of the HBC core and of the HOPG substrate with predominantly σ-symmetry. (Some of these features are not shown in Figure 6 since we have restricted the scale mainly to the π-peaks). The shoulder at 5 eV and the broad main peak at about 8.2 eV correspond to states of the HBC core, while the shoulders at 6.5 and 10.4 eV correspond to states of the alkyl chains and/or the graphite substrate. These assignments are based not only on the results of the quantum chemical calculations, but also by a comparison of the results presented here with similar results for unsubstituted HBC molecules on HOPG,[26] for the bare HOPG substrate (see Figure 6c), and for a sample of HBC-C_{12} spin-coated on HOPG (not shown here).

The strong angle dependence of the π-features in Figures 6a and 6b can be interpreted in terms of a high degree of molecular orientation of the HBC cores with respect to the surface. The solid lines are recorded with p-polarized light, where $\vec{\mathbf{E}}$ is in the plane of the incoming light and the surface normal, with an incident angle of $\alpha = 60°$ and an electron takeoff angle of $\theta = 30°$ (see inset in Figure 6). In that geometry the two π-peaks are strongly resolved. The comparison with the HOPG spectrum in Figure 6c shows that these features are not associated with the HOPG substrate. Changing the geometry to a case where $\vec{\mathbf{E}}$ is oriented parallel and the detector within the surface (unfilled circles in Figures 6a and 6b), the π-features 1 and 2 vanish completely. This behavior can be explained using eq. 1a in Figure 5: if the $\vec{\mathbf{E}}$ vector is oriented parallel to the molecular plane $m_{x,y}$ and the detector is positioned within the plane, then for all transitions from π-orbitals the matrix-element $M_{f,I}$ vanishes. This means that $m_{x,y}$ must be oriented parallel to the

basal plane of the surface. Therefore, this angular dependence can be interpreted in terms of a packing of HBC cores oriented parallel to the substrate. It should be mentioned that in these measurements the sample was slightly tilted toward the detector in order to increase the electron flux in its direction. Both, $\vec{E}$ and the detector position were about 5° out of the surface plane ($\omega = 5°$). In the last set of curves (plotted with unfilled squares) $\vec{E}$ is oriented parallel to the surface, as in the case of the spectra plotted with the unfilled circles. However, here the detector is positioned out of the molecular plane by $\theta = 30°$, which again allows us to detect electrons excited from π-orbitals again. The two peaks are only slightly visible within the spectra.

It should be noted that the basal plane of the HOPG surface is polycrystalline, with a size of the single domains on the micrometer scale (see black arrows Figure 4), while the spot of the synchrotron light irradiating the sample is on the millimeter and sub-millimeter range. On each HOPG domain, the molecules exhibit an orientation that is induced by the lattice of the substrate. Consequently, since the ARUPS spectra are averaged over such large areas, it is assumed that the molecules are lying flat on the substrate surface but laterally not oriented. While an azimuthal order of the molecules over domain boundaries in such a large region is very unlikely, this should have a little effect on the angular dependence of the ARUPS spectra. In fact, also in this case the π-features would disappear when the spectra are recorded in the same geometry as used for the spectra shown with unfilled circles in Figure 6 (s-polarized light; $a = 60°$, $q = 90°$, $f = 90°$). This absence of the π-features clearly indicates a flat adsorption of the molecules on the surface within the area irradiated in the ARUPS experiment. On the other hand, it is not possible that a film with lateral order, but azimuthal disorder could lead to the observed orientation dependence, as shown in Figure 6 in which both π-features are simultaneously affected when the geometry is particularly changed. Nevertheless, it is fair to point out that the ARUPS does not provide insight into the lateral arrangement of the molecules.

Furthermore, upon thermal annealing (at 425 K for 1 h) the orientation dependence of the spectra enhances (Figure 6b). This result is in good agreement with the presence of the "mesophase", which it is known to exist between 333 and 672 K, where the molecules tend to stack in columnar aggregates.[19]

So far we have discussed the growth of ordered films of HBC-C_{12} on HOPG prepared using solutions with very low molecular concentrations. Except for the case of the spin-coating film of Figure 2, only the rate of physisorption was varied. Next, the concentration of the solution was changed. Figure 7 shows ARUPS spectra of a film prepared by procedure (C). Here, the solution used had a concentration, which corresponds to 50 molecular layers. The π-region of the ARUPS spectrum of the as-prepared sample (Figure 7a) exhibits only a big unstructured shoulder instead of the two π-peaks resolved in the case of the thinner film (as shown in Figure 6). After annealing, the typical HBC π-features 1 and 2 are resolved (Figure 7b), but the angle-dependence of these structures is less pronounced compared to the thin film (Figure 6b). This indicates either a lower degree of azimuthal order in a thick film compared to the thin one or—alternatively —an ordered thick adsorbate film consisting of molecules oriented nonparallel to the substrate surface. However, it is not clear if there is a structural transition of the Stransky-Krastanov type within the film, such that the molecules of the undermost layers are still oriented parallel to the substrate surface whereas the outermost layers are less-azimuthaly ordered, or, have a different azimuthal order. This question is under investigation and will be the subject of future studies.

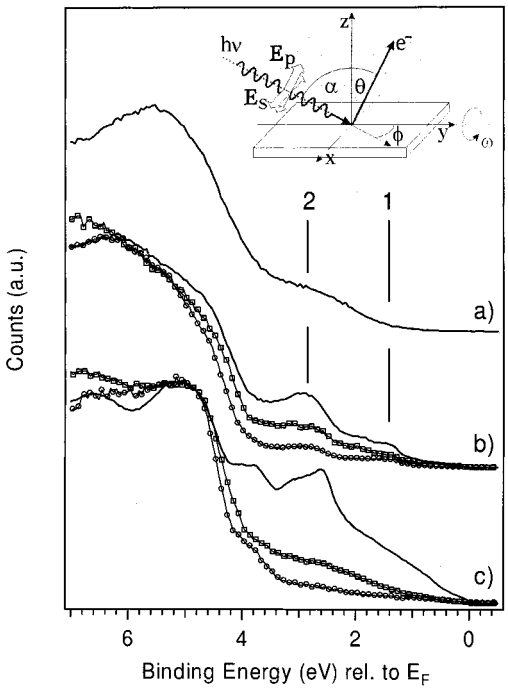

Figure 7. ARUPS spectra of samples prepared by slow casting of 50 layers, recorded at the same geometries as used in the spectra of Figure 6 (see description in the figure caption of Figure 6). (a) As-prepared; (b) thermal annealed at 425 K for 1 h, and (c) of freshly cleaved HOPG. The spectra were plotted relative to the Fermi level; the photon energy was $h\nu = 85$ eV.

Conclusions

Well-defined, ordered HBC-C_{12} films are formed on HOPG surfaces by self-assembly from solution. The morphology of the molecular layered films with a thickness in the monolayer regime may be controlled by tuning the rate of evaporation of the solvent. Both SFM images and the polarization-dependence of the π-features in the valence band spectra suggest that alkyl-substituted hexa-*peri*-hexabenzocoronene molecules lie flat on the HOPG surface. These results indicate that growth into layered architectures is a kinetically governed phenomenon, leading to the formation of hetero-epitaxial crystallites on the organic thin film. In the framework of future molecular electronics applications, these findings represent a step forward toward the development of molecular wires consisting of π-conjugated disks stacked on a conductive electrode.

Acknowledgment. The authors are grateful to Dr. N. Severin for the Molecular Mechanics modeling. The work was supported by TMR project SISITOMAS (project number 0261) and Volkswagen-Stiftung. P.S. acknowledges the EU for a TMR grant. Research on condensed molecular solids and polymers in Linköping is supported in general by grants from the Swedish Natural Science Research Council (NFR), the Swedish Research Council for Engineering Sciences (TFR), another European Commission TMR network (project number 1354 SELOA), and a Brite/EuRam contract BRPR-CT97-0469 (project number 4438 OSCA).

References and Notes

(1) Lehn, J.-M. *Supramolecular Chemistry—Concepts and Perspectives*; VCH: Weinheim, 1995.

(2) Percec, V.; Ahn, C.-H.; Ungar, G.; Yeardley, D. J. P. M.; Möller, M.; Sheiko, S. S. *Nature* **1998**, *391*, 161.

(3) Stocker, W.; Karakaya, B.; Schürmann, B. L.; Rabe, J. P.; Schlüter, A.-D. *J. Am. Chem. Soc.* **1998**, *120*, 7691.

(4) Burroughes, J. H.; Bradley, D. D. C.; Brown, A. R.; Marks, R. N.; Mackay, K.; Friend, R. H.; Burns, P. L.; Holmes, A. B. *Nature* **1990**, *347*, 539.

(5) Garnier, F.; Horowith, G.; Peng, X.; Fichou, D. *Adv. Mater.* **1990**, *2*, 592.

(6) Friend, R. H.; Gymer, R. W.; Holmes, A. B.; Burroughes, J. H.; Marks, R. N.; Taliani, C.; Bradley, D. D. C.; Dos Santos, D. A.; Brédas, J. L.; Lögdlund, M.; Salaneck, W. R. *Nature* **1999**, *397*, 121.

(7) Bumm, L. A.; Arnold, J. J.; Cygan, M. T.; Dunbar, T. D.; Burgin, T. P.; Jones, L., II; Allara, D. L.; Tour, J. M.; Weiss, P. S. *Science* **1996**, *271*, 1705.

(8) Dhirani, A.; Zehner, R. W.; Hsung, R. P.; Guyot-Sionnest, P.; Sita, L. R. *J. Am. Chem. Soc.* **1996**, *118*, 3319.

(9) Forrest, S. R.; Burrows, P. E.; Haskal, E. I.; So, F. F. *Phys. Rev. B* **1994**, *49*, 11309.

(10) Biscarini, F.; Zamboni, R.; Samorí, P.; Ostoja, P.; Taliani, C. *Phys. Rev. B* **1995**, *52*, 14868.

(11) Soukopp, A.; Glöcker, K.; Kraft, P.; Schmitt, S.; Sokolowski, M.; Umbach, E.; Mena-Osteritz, E.; Bäuerle, P.; Hädicke, E. *Phys. Rev. B* **1998**, *58*, 13882.

(12) Samorí, P.; Francke, V.; Müllen, K.; Rabe, J. P. *Chem. Eur. J.* **1999**, *5*, 2312.

(13) Smolenyak, P.; Peterson, R.; Nebesny, K.; Törker, M.; O'Brien, D. F.; Armstrong, N. R. *J. Am. Chem. Soc.* **1999**, *121*, 8628.

(14) Alivisatos, A. P.; Barbara, P. F.; Castleman, A. W.; Chang, J.; Dixon, D. A.; Klein, M. L.; McLendon, G. L.; Miller, J. S.; Ratner, M. A.; Rossky, P. J.; Stupp, S. I.; Thompson, M. E. *Adv. Mater.* **1998**, *10*, 1297.

(15) Kelley, T. W.; Granstrom, E. L.; Frisbie, C. D. *Adv. Mater.* **1999**, *11*, 261.

(16) Metzger, R. M. *Acc. Chem. Res.* **1999**, *32*, 950.

(17) Stabel, A.; Herwig, P.; Müllen, K.; Rabe, J. P. *Angew. Chem., Int. Ed. Engl.* **1995**, *34*, 1609.

(18) Müller, M.; Kübel, C.; Müllen, K. *Chem. Eur. J.* **1998**, *4*, 2099.

(19) Herwig, P.; Kayser, C. W.; Müllen, K.; Spiess, H. W. *Adv. Mater.* **1996**, *8*, 510.

(20) Iyer, V. S.; Yoshimura, K.; Enkelmann, V.; Epsch, R.; Rabe, J. P.; Müllen, K. *Angew. Chem., Int. Ed. Engl.* **1998**, *37*, 2696.

(21) Bustamante, C.; Keller, D. *Phys. Today* **1995**, *48*, 12, 32.

(22) Takano, H.; Kenseth, J. R.; Wong, S. S.; O'Brien, J. C.; Porter, M. D. *Chem. Rev.* **1999**, *99*, 2845.

(23) Finot, M. O.; McDermot, M. T. *J. Am. Chem. Soc.* **1997**, *119*, 8564.

(24) Digital Instruments, Santa Barbara, CA.

(25) Done using DISCOVER VERSION 4.0.0, Biosym Technologies Inc., San Diego, CA. Insights into the molecular mechanics calculations can be found in: Drexler, K. E. *Nanosystems—Molecular Machinery, Manufacturing and Computation*; J. Wiley & Sons: New York, 1992.

(26) Bässler, M.; Forsell, J.-O.; Björneholm, O.; Feifel, R.; Jurvansuu, M.; Aksela, S.; Sundin, S.; Sorensen, S.; Nyholm, R.; Ausmees, A.; Svensson, S. *J. Electron Spectrosc. Relat. Phenom.* **1999**, *101−103*, 953.

(27) Keil, M.; Samorí, P.; dos Santos, D. A.; Kugler, T.; Stafström, S.; Brand, J. D.; Müllen, K.; Brédas, J. L.; Rabe, J. P.; Salaneck, W. R. *J. Phys. Chem. B* **2000,** *104*, 3967.

(28) Güntherodt, H.-J.; Wiesendanger, R. *Scanning Tunneling Microscopy I.*; Springer-Verlag: Berlin, 1992.

(29) Hooks, D. E.; Fritz, T.; Ward, M. D. *Adv. Mater.* **2001**, *13*, 227.

(30) Palermo, V.; Biscarini, F.; Zannoni, C. *Phys. Rev. E* **1998**, *57*, R2519.

(31) Brundle, C. R.; Baker, A. D. *Electronic Spectroscopy*; Academic Press: New York, 1977; Vol. 1.

(32) Steinrück, H. P. *J. Phys. Condens. Matter.* **1996**, *8*, 6465.